ACS APPLIED POLYMER MATERIALS

pubs.acs.org/acsapm

Article

Thermoresponsive Modular Nano-Objects Via RAFT Dispersion Polymerization in a Non-Polar Solvent

Gianmaria Gardoni, Nicolò Manfredini, Mattia Monzani, Mattia Sponchioni,* and Davide Moscatelli

Cite This: *ACS Appl. Polym. Mater.* 2023, 5, 494−503

Read Online

ACCESS | Metrics & More | Article Recommendations | Supporting Information

ABSTRACT: Thermoresponsive polymer nano-objects able to dynamically change their morphology in response to modifications in the local temperature are finding growing attention for biomedical, optical, and oil & gas applications. This smart behavior can be accessed by precisely controlling the microstructure of AB block copolymers, which can be obtained by leveraging the pseudoliving character of the reversible addition−fragmentation chain transfer (RAFT) polymerization. Most of the examples reporting the synthesis of highly controlled thermoresponsive nano-objects via RAFT dispersion polymerization currently refer to aqueous systems. However, the possibility of synthesizing thermoresponsive copolymers with a well-defined phase separation and bulk response in organic solvents is becoming more and more critical for applications in the oil & gas field and in lubricants for heat engines. In this study, we propose a convenient strategy for synthesizing modular thermoresponsive block copolymers dynamically self-assembling into nano-objects with different morphologies in the hydrocarbon blend dectol (50:50% v/v decane/toluene). Two macromolecular chain transfer agents (macroCTAs) with different degree of polymerization were synthesized from lauryl methacrylate. The chain extension of these macroCTAs with di(ethylene glycol) methyl ether methacrylate via RAFT dispersion polymerization led to copolymers forming, when the temperature is lowered below their cloud point, nano-objects whose morphology could be controlled by modulating the solid content of the formulation and the length of both blocks in the copolymer. We also revealed how the phase-separation temperature and bulk response is influenced by these same parameters, allowing us to tune the material response to the needs of the final application.

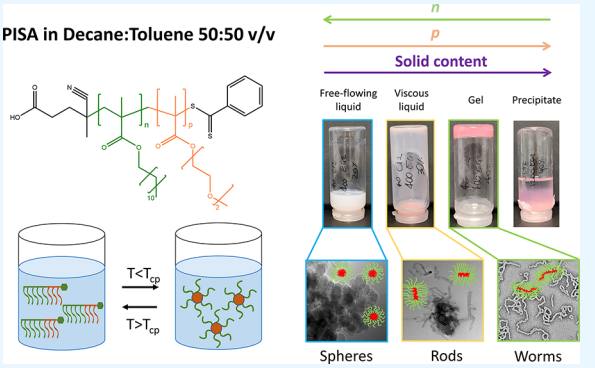

KEYWORDS: *polymeric nano-objects, emulsion polymerization, non-polar media, RAFT, thermoresponsive polymers, UCST, phase diagram*

1. INTRODUCTION

Free-radical emulsion polymerization (FRPe) is a versatile technique allowing for the production of nanostructured polymer-based materials that we encounter in our daily life, including coatings, paints, adhesives, and personal care products.[1−3] However, FRPe only provides poor control over the microstructure of the final polymer. Therefore, it hampers the production of nano-objects with specific morphology and predetermined size, useful in advanced applications like drug delivery, optics, or cosmetics.[4−7]

In this context, the reversible addition−fragmentation chain transfer (RAFT) polymerization offers an important alternative when high control over the polymer composition and microstructure is required.[8,9] An important example is represented by the possibility of synthesizing well-defined block copolymers with high blocking efficiency, poor interchain compositional drift, and organized into nano-objects both in organic and aqueous solvents via RAFT polymerization-induced self-assembly (PISA).[10−13] The outstanding level of control over the structure of the copolymer offered by this pseudoliving polymerization proved to be decisive in the fine modulation of important properties of the produced nano-objects, including their morphology, average size, and, more recently, their phase separation in response to thermal stimuli.[14−17] As a matter of fact, the so-called thermoresponsive polymers are interesting materials able to sharply and often reversibly change their miscibility with a given solvent at a critical temperature, generally called cloud point (T_{cp}).[18,19] According to how their solubility changes with temperature, these materials can be divided into polymers with a Lower or Upper Critical Solution Temperature (LCST or UCST) if they become more insoluble in the outer phase with increasing or decreasing temperature, respectively.[20−23] By starting from this general concept, it was

Received: September 13, 2022
Accepted: November 28, 2022
Published: December 8, 2022

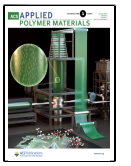

Scheme 1. Schematic Representation of the Synthesis of Thermoresponsive Nano-Objects with Three Degrees of Freedom, Namely, *n*, *p*, and Solid Content, through the Combination of RAFT Solution and Dispersion Polymerization in Organic Solvent[a]

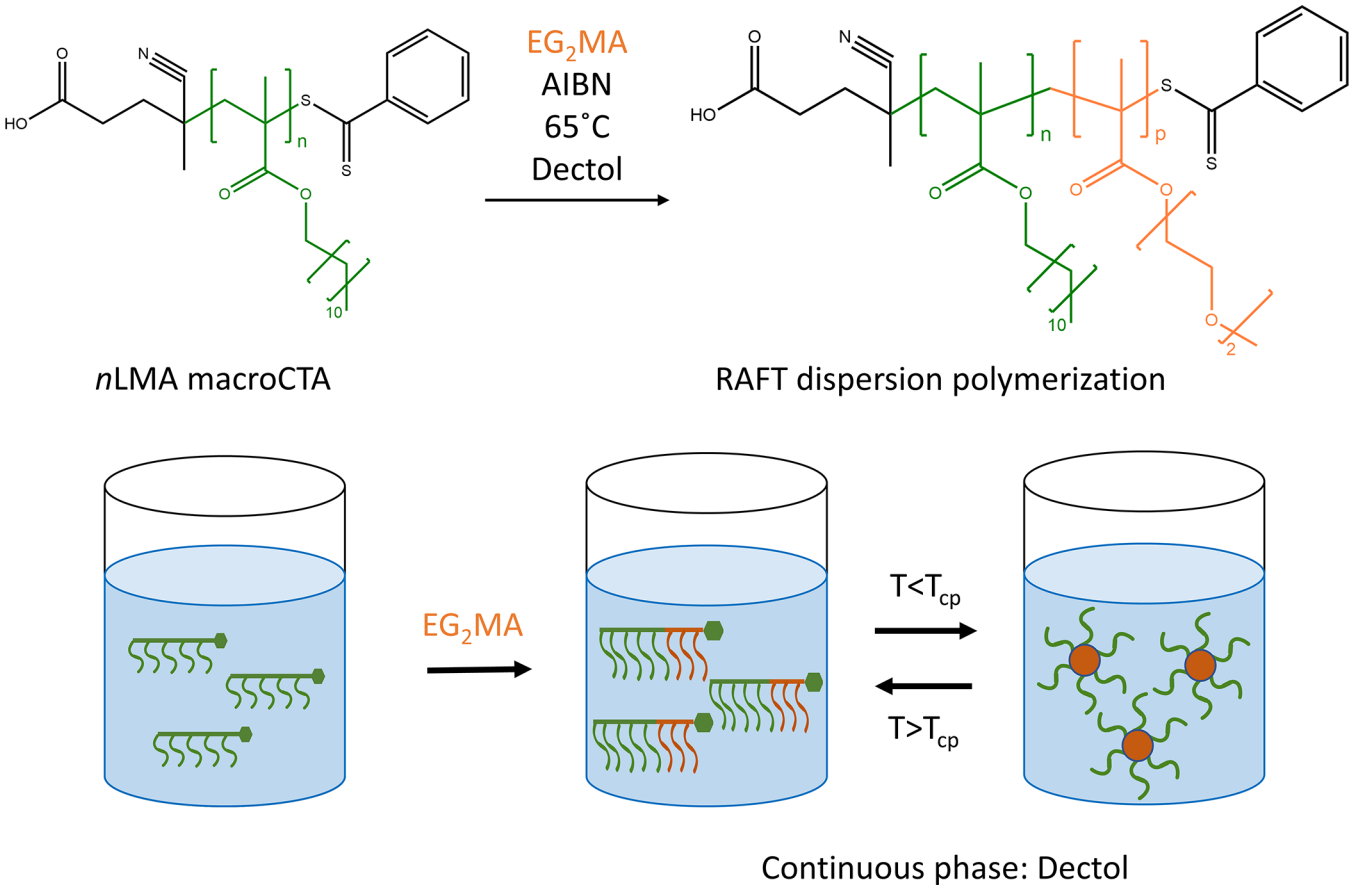

[a]In this work, two macroCTAs with n = 20 and 40 were synthesized with LMA as oil-soluble monomer (green). Each one was chain-extended with EG_2MA (orange) via RAFT dispersion polymerization targeting p = 400, 600, 800, 1000, and 1200. Finally, three solid contents were investigated, namely, 20, 30, and 40% w/w.

demonstrated that the bulk response of formulations of these smart materials depends upon the polymer microstructure. In particular, block copolymers comprising a solvophilic segment and a thermoresponsive one can undergo a reversible self-assembly into nano-objects, whose morphology is dictated, as for low molecular weight surfactants, by the packing parameter.[24] The most reported morphologies are worms, spheres, or vesicles, which in turn greatly influence the macroscopic behavior of the dispersion and its possible applications.[25,26]

Despite the great potential and interest toward thermoresponsive nanostructured materials, the majority of the examples available in the literature refers to waterborne systems. This is ascribed to their intrinsic biocompatibility, essential for polymers in the biomedical field, where the thermoresponsive behavior is greatly and efficiently exploited.[21,27−34]

However, RAFT dispersion polymerization is a versatile technique that was applied in organic solvents with excellent results and interesting applications, such as for the synthesis of stabilizers for water/oil/water (w/o/w) emulsions and of lubricants for engine oils.[11,35−40]

In this work, well-defined diblock copolymers with a UCST have been synthesized via RAFT dispersion polymerization in a poorly polar solvent, *i.e.*, a 50:50% v/v decane/toluene hydrocarbon blend (dectol). This solvent was chosen as a model oil, able to simulate both the paraffinic and aromatic fraction of crude oil and hence particularly suitable for screening polymer additives aimed at oil & gas applications.[41,42] The oil-soluble macromolecular chain transfer agent (macroCTA), deputed to provide colloidal stability to the system, was synthesized from lauryl methacrylate (LMA) via RAFT solution polymerization. This macroCTA was chain-extended with di(ethylene glycol) methyl ether methacrylate (EG_2MA), which exhibits a thermoresponsive behavior in the chosen solvent. Indeed, polyEG_2MA is mostly known for its LCST behavior in water,[43,44] but we found out that it behaves like a UCST-type polymer in dectol, as it is insoluble at low temperatures and becomes soluble above a characteristic critical temperature (T_{cp}). Therefore, the addition of a polymeric block with an upper critical solution temperature leads to copolymers soluble in dectol at temperatures higher than the cloud point (T_{cp}, controllable in the range of 57−72°C) and able to rearrange spontaneously into nano-objects as soon as the temperature is decreased below the T_{cp}. As expected, we discovered that the morphology of these nano-objects is a function of the number of units in the stabilizing (n in Scheme 1) and in the core-forming (p in Scheme 1) blocks of the copolymer as well as of its concentration. To elucidate the role of these degrees of freedom, precisely controllable via RAFT polymerization, a library of diblock copolymer formulations was produced, and its thermoresponsive behavior was studied. In detail, two macroCTAs with n = 20 and 40 were produced, and

https://doi.org/10.1021/acsapm.2c01598
ACS Appl. Polym. Mater. 2023, 5, 494−503

each one was chain-extended with EG_2MA to obtain p in the range of 400−1200 at different solid contents from 20 to 40% w/w. This allowed us to highlight the phase diagram for these block copolymers, showing that different morphologies, including spheres, worms, and vesicles, can be targeted by acting on the reaction parameters. In particular, the formation of worms below the T_{cp} allows for a temperature-driven thickening or, in some cases, gelation of the system, an interesting property that can be relevant in specific applications.

2. EXPERIMENTAL SECTION

2.1. Materials. Decane (DEC, ≥99%, MW = 142.28 g/mol, Sigma-Aldrich), toluene (TOL, ≥99.5%, MW = 92.14 g/mol, Sigma-Aldrich), di(ethylene glycol)methyl ether methacrylate (EG_2MA, MW = 188.2 g/mol, Sigma-Aldrich), 2,2′-azobis(2-methylpropionitrile) (AIBN, ≥98%, MW = 164.21 g/mol, Sigma-Aldrich), lauryl methacrylate (LMA, 96%, MW = 254.41 g/mol, Sigma-Aldrich), chloroform ($CHCl_3$, ≥99%, MW = 119.38 g/mol, Sigma-Aldrich), ethanol (EtOH, ≥99.8%, MW = 46.07 g/mol, Sigma-Aldrich), 4-cyano-4-(phenylcarbonothioylthio) pentanoic acid (CPA, MW = 279.38 g/mol, Sigma-Aldrich), distilled H_2O, tetrahydrofuran (THF, 99.9%, MW = 72.11 g/mol, Sigma-Aldrich), chloroform-*d* ($CDCl_3$, ≥99.8%, MW = 120.38 g/mol, Sigma-Aldrich), deuterated dimethyl sulfoxide (DMSO-d_6, ≥99.7%, MW = 78.13 g/mol, Sigma-Aldrich), deuterium oxide (D_2O, 99.9%, MW = 20.03 g/mol, Sigma-Aldrich) were of analytical-grade purity and used as received unless otherwise noted.

2.2. Synthesis of the Oil-Soluble MacroCTAs. LMA was polymerized via RAFT solution polymerization to obtain oil-soluble polymers with different chain lengths. In particular, two macroCTAs were produced by setting the ratio between the monomer and CPA mole concentrations (n in Scheme 1) to 20 and 40. These two macroCTAs will be referred to as 20LMA and 40LMA, respectively.

As an example, to synthesize the 20LMA, 4 g of LMA (15.7 mmol) and 0.22 g of CPA (0.8 mmol, *i.e.*, n = 20) were dissolved in 38.6 mL of chloroform in a 100 mL round-bottom flask equipped with a magnetic stirrer. Then, the solution was purged with nitrogen for 20 min at room temperature and heated to 65 °C in an oil bath under magnetic stirring. To initiate the reaction, 43 mg of AIBN (0.26 mmol, one-third molar ratio with respect to CPA) were dissolved in 1 mL of chloroform and added to the reaction mixture, which was left to react for 24 h with a condenser in order to prevent the evaporation of the solvent. Considering initiator, CPA, and monomer, the solid content was equal to 10% w/w.

After the process, the polymer was precipitated in an excess of EtOH (9:1 ratio in volume) and centrifuged for 6 min at 6000 rpm. The upper phase containing the unreacted monomer was removed, while the lower phase was dried under a flux of air. Finally, the polymers were recovered as viscous red liquids and stored at −20 °C.

The obtained macroCTAs were characterized before and after the purification process via nuclear magnetic resonace (NMR) spectroscopy by dissolving 10 mg of the sample in 0.7 mL of $CDCl_3$ to determine the monomer conversion and degree of polymerization. The analysis was performed on a Bruker 400 MHz spectrometer, with 64 scans per measurement. Moreover, the samples were analyzed via gel permeation chromatography (GPC) on a Jasco LC-2000Plus apparatus. For the GPC analysis, 4 mg of polymer were dissolved in 1 mL of THF and filtered through a 0.45 μm polytetrafluoroethylene (PTFE) membrane before injection. The instrument comprised three styrene/divinylbenzene columns (Polymer Standard Service; pore sizes 10^3, 10^5, and 10^6 Å; 300 mm length and 8 mm internal diameter) and a precolumn (50 mm length and 8 mm internal diameter), paired with a refractive index (RI) detector to record the signal. The separation was performed using THF as eluent at 35 °C with a flow rate of 1 mL/min. Through GPC analysis, it was possible to assess the molecular weight distribution (MWD) based on a calibration made with polystyrene standards from 580 to 3250 000 Da (Polymer Laboratories).

2.3. Synthesis of Thermoresponsive Block Copolymers. The synthesized poly(LMA) macroCTAs were chain-extended with EG_2MA to grow a thermoresponsive block able to make the copolymer to self-assemble into nano-objects with different morphologies according to controllable parameters such as solid content and number of solvophilic and solvophobic units.

These diblock copolymers were prepared via RAFT dispersion polymerization in dectol (a 50/50% v/v mixture of toluene and decane) by targeting different degrees of polymerization of EG_2MA (p), achieved by modulating the molar ratio between EG_2MA and the nLMA macroCTA.

In particular, EG_2MA was used to produce copolymers with increasing p, from 400 to 1200, and the reactions were performed with different solid content, from 20% up to 40%. Hereinafter, these diblock copolymers will be referred to as nLMA-$p$$EG_2MA$, to highlight the tuned process parameters. As an example, to synthesize 40LMA-600EG_2MA, 1.5 g of EG_2MA (8 mmol) and 0.14 g of 40LMA (13 μmol, *i.e.*, EG_2MA/LMA = 600 mol/mol) were dissolved in 6.6 g of dectol in a 50 mL round-bottom flask equipped with a magnetic stirrer. The solution was then purged with nitrogen for 30 min at room temperature and placed in an oil bath at 65 °C. Subsequently, 0.73 mg of AIBN (4 μmol, *i.e.*, AIBN/40LMA = 0.33 mol/mol) was dissolved in 0.5 g of dectol and injected in the flask to initiate the reaction, which was left to proceed for 21 h.

The final product was analyzed via NMR and GPC, to determine the conversion of EG_2MA, p, CTA efficiency, and the MWD of the copolymer. The analytical procedures are reported in the previous section.

The nanoparticle (NP) cloud point (T_{cp}), volume-average diameter (Dv), and polydispersity index (PDI) were assessed via dynamic light scattering (DLS) on a Malvern Zetasizer Nano ZS instrument at a scattering angle of 173°. The samples were first heated to 80 °C for 2 h and then equilibrated at 25 °C in a water bath with temperature controlled through a heating plate and a thermocouple. Finally, they were diluted to 0.5% w/w in dectol before the analysis, and the measurements were performed in triplicate. For the determination of T_{cp}, the samples were heated and cooled in a specific temperature range (50−65 °C), and both the NP size and relative scattering intensity (RSI) were measured every 1 °C, with an equilibration time of 5 min before each measurement. In particular, T_{cp} was considered as the inflection point of the size vs temperature curve.

Eventually, for a temperature below the cloud point (*e.g.*, 25 °C) a phase diagram was built, and transmission electron microscopy (TEM) was employed to visually assess the morphology of the nano-objects in the different regions of the diagram. TEM micrographs were acquired with a Philips CM200 electron microscope at 200 kV, equipped with a field emission gun filament. The samples were diluted to 0.1% w/w in dectol, and 30 μL of the dispersion, after being carefully mixed, was deposited onto a 200 mesh carbon-coated copper grid and dried. A Gatan US 1000 CCD camera was used, and 2048 Å ∼ 2048 pixel images with 256 gray levels were recorded.

Rheological measurements were performed using a rotational rheometer (AR-1500 TA Instruments) coupled to a 20 mm flat-plate geometry at different temperatures, namely, 25 and 90 °C. The storage component (G', Pa) and loss component (G'', Pa) were determined by a strain sweep test ranging from 0.1 to 100% at an oscillatory frequency of 10 rad/s with a gap between plates equal to 1 mm.

3. RESULTS AND DISCUSSION

3.1. Oil-Soluble MacroCTAs. First, two oil-soluble macroCTAs based on poly(lauryl methacrylate) were synthesized via RAFT solution polymerization in chloroform. The employment of a pseudoliving polymerization technique allowed us to control the number of LMA units incorporated in the final polymer and therefore the degree of polymerization (n), which was set to 20 and 40. In this way, it was possible to carefully vary one of the three degrees of freedom considered in this work and obtain macroCTAs with different stabilizing properties.

The products have been characterized in terms of average chain length, molecular weight distribution, and monomer

https://doi.org/10.1021/acsapm.2c01598
ACS Appl. Polym. Mater. 2023, 5, 494−503

conversion. These properties are summarized in Table 1 and are complemented by the GPC chromatograms in Figure S1 and the

Table 1. Conversion (χ), n, Number-Average Molecular Weight (Mn), and Dispersity ($Đ$) of the nLMA macroCTAs

sample	χ (%)	n [-]	Mn [Da]	$Đ$ [-]
20LMA	95.2	23	4200	1.16
40LMA	89.3	40	9000	1.14

NMR spectrum shown in Figure S2. In particular, the actual degree of polymerization n of lauryl methacrylate was computed according to eq. S1. Thanks to the pseudoliving feature of the RAFT polymerization, it was possible to synthesize macroCTAs with narrow molecular weight distribution (i.e., $Đ < 1.2$), and n close to the desired value (Table 1). Moreover, in both the syntheses, high LMA conversions (>89%), as determined via NMR according to eq. S2, could be obtained.

3.2. Modular Diblock Copolymers. After having confirmed the possibility of obtaining macroCTAs with controllable chain length and narrow MWD, these were chain-extended with EG_2MA via RAFT dispersion polymerization in dectol to produce well-defined diblock copolymers with tunable microstructure.

The polymerization kinetics for the sample 20LMA-600EG_2MA was tracked via NMR and is shown in Figure 1 in

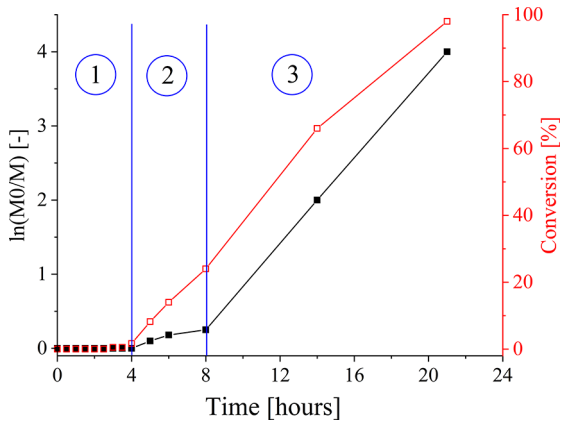

Figure 1. $\ln(M_0/M)$ and conversion as a function of time for one of the RAFT dispersion syntheses in dectol (i.e., 23LMA-600EG2MA at 20% w/w).

terms of $\ln(M_0/M)$ versus time, where M_0 and M are the monomer concentration at time zero and at the considered time point, respectively. Here, three different regimens can be clearly distinguished, as it is typical of the RAFT dispersion polymerization.[45] In particular, an induction period was observed during the first 4 h of the process. This was followed by an increase in the polymerization rate until 8 h, ascribed to a homogeneous polymerization occurring in the bulk and finally followed by micellar nucleation. This caused an increase in the monomer concentration in the solvophobic microenvironment represented by the micelle core and was thus responsible for the drastic increase in the polymerization rate, which led to monomer conversion greater than 90% after 21 h. The linear increase in $\ln(M_0/M)$ during time suggests a constant radical concentration in the system, a typical feature of the RAFT polymerization. This confirms its good control throughout the three phases of the process.

Based on these preliminary results, we synthesized a library of modular diblock copolymers by independently modulating three degrees of freedom. In particular, we tested two chain lengths for the solvophilic block n, equal to 20 and 40, different degrees of polymerization for the thermoresponsive block p, namely, 400, 600, 800, 1000, and 1200, and three different dry contents 20, 30, and 40% w/w. The products were characterized via GPC to determine the MWD. ^{1}H NMR instead allowed us to determine the actual p and the EG_2MA conversion, according to eqs. S3 & S4. An illustrative NMR spectrum, instrumental for showing the characteristic peaks considered during the analysis, is shown in Figure S3 for the sample 40LMA-600EG_2MA. The properties measured for all the diblock copolymers in terms of monomer conversion, p, CTA efficiency, and MWD are summarized in Tables S1−S3 for the three different solid contents.

High monomer conversions have been achieved in dectol, with the final copolymers having a measured p close to the target one. This confirms the possibility of reliably controlling the number of EG_2MA units incorporated in the thermoresponsive portion, a useful tool to modulate the physicochemical properties of the nano-objects produced.

In addition, the GPC chromatograms, reported in Figure 2a for the copolymers produced at 20% w/w and with n = 40, confirm high blocking efficiency and narrow MWDs for these copolymers. The small high-molecular-weight shoulders recorded for the different samples can be ascribed to the formation

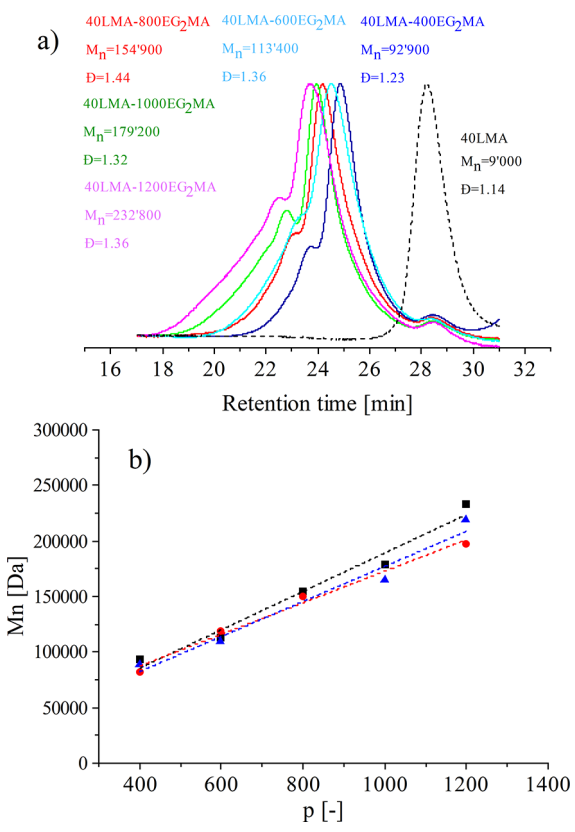

Figure 2. (a) GPC chromatograms for the 40LMA-pEG_2MA 20% w/w syntheses. (b) Mn vs p for the 40LMA-pEG2MA 20% (black squares), 30% (red circles), and 40% (blue triangles) copolymers. The dashed lines represent the linear fits of the experimental data, obtained with R^2 = 0.9728 (20% syntheses), R^2 = 0.9885 (30% syntheses), and R^2 = 0.9771 (40% syntheses).

https://doi.org/10.1021/acsapm.2c01598
ACS Appl. Polym. Mater. 2023, 5, 494−503

of cross-linked polymer, due to the presence of dimethacrylate impurities in the commercial EG_2MA.[46] As expected, the copolymer number-average molecular weight (Mn) increases linearly with the measured p according to eq 1.

$$Mn_{copolymer} = \chi_{EG2MA} \times p \times M_{EG2MA} + Mn_{poly(LMA)} \quad (1)$$

Here, χ_{EG2MA} is the monomer conversion, $Mn_{copolymer}$ and $Mn_{poly(LMA)}$ are the number-average molecular weights of the final copolymer and of the macroCTA, respectively, while M_{EG2MA} is the molecular weight of EG_2MA. The theoretical trend deduced from eq 1 was experimentally confirmed by the linear increase in molecular weight of the copolymers with p at all the investigated solid contents, as shown in Figure 2b for n = 40. Similar trends were observed for the copolymers with n = 20 (see Figure S4).

Overall, well-defined diblock copolymers with controllable n and p could be produced at different dry contents via RAFT dispersion polymerization in a hydrocarbon blend, confirming the great versatility of this technique in a non-polar medium and its good control over the polymerization.

3.3. Thermoresponsive Behavior and Phase Diagram. Starting from the obtained modular diblock copolymers with controllable microstructure, we investigated the thermoresponsive behavior of these materials. In particular, the diblock copolymers are expected to show a UCST-like behavior in dectol. Indeed, in this non-polar solvent, poly(EG_2MA) is soluble at high temperatures and phase separates from the solution as the temperature is decreased below the T_{cp} (see Figure S5). In this configuration, the oil-soluble poly(LMA) provides colloidal stability to the formed nano-objects, whose morphology is dependent on the copolymer microstructure and solid content.

To demonstrate this thermoresponsive behavior, the average size and relative scattering intensity (RSI) were tracked by DLS at increasing temperature, as shown in Figure 3a for the sample 40LMA-600EG_2MA, as an example. The RSI is a useful parameter, since it is proportional to the NP concentration and size at the sixth power.[47] Therefore, its decrease testifies a progressive solubilization of the copolymer and provides a useful indication of the phase separation. A steep decrease in both size and RSI was experienced for this sample in proximity of a temperature of 57 °C.

The temperature in correspondence of these phenomena was taken as the cloud point for that specific diblock copolymer. The same procedure was repeated for each 40LMA-$p$$EG_2MA$ copolymer, and the cloud points measured were collected and plotted as a function of p in Figure 3b. This highlights a linear dependence between the length of the thermoresponsive block and the cloud points of the copolymers, which can then be finely tuned in a wide range (*i.e.*, from 57 up to 72 °C) by targeting the desired p through RAFT polymerization.

Intriguingly, the phase separation below the cloud point led to different bulk behaviors depending upon n, p, and solid content. To highlight this dependency, two phase diagrams were created by fixing a temperature below the cloud point (25 °C) and analyzing the macroscopic behavior of both 23LMA-$p$$EG_2MA$ and 40LMA-$p$$EG_2MA$ dispersions as a function of p and solid content (Figure 4a,b).

From the graphs, it is possible to notice four different regions defined by the parameters considered and associated to the following behaviors: (i) free-flowing cloudy liquid, (ii) viscous cloudy dispersion, (iii) self-standing clear gel, and (iv) precipitation of a polymer-rich phase from dectol. The visualization of these four macroscopic behaviors is available in Figure S6.

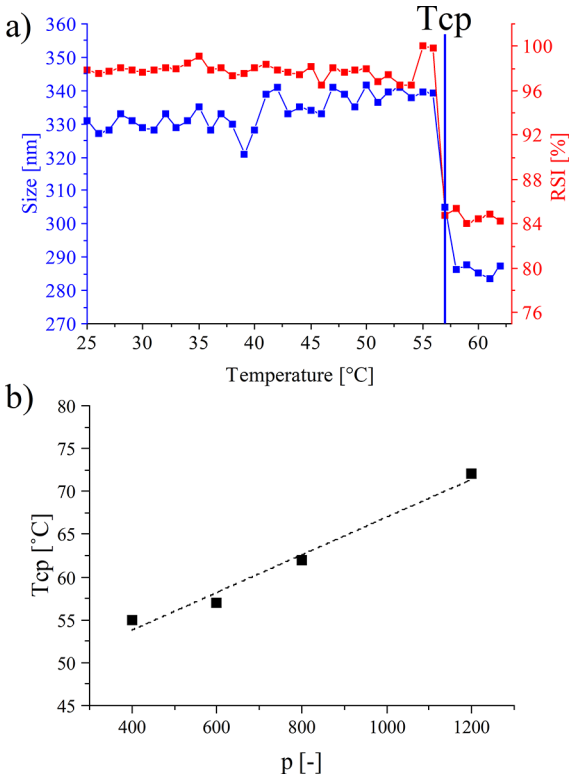

Figure 3. (a) Volume-average size and RSI measured via DLS for the copolymer 40LMA-600EG_2MA at 30% w/w. The T_{cp} was determined from this plot as the value where both size and RSI curves reached an inflection point at increasing temperature. (b) Linear correlation between the T_{cp} and the length of the thermoresponsive block for 40LMA-pEG_2MA copolymers at 30% w/w. The dashed line represents the best fit of the experimental data, with R^2 = 0.98.

The two diagrams are slightly different due to the greater stability provided by the longer macroCTA in the case of the 40LMA-$p$$EG_2MA$ copolymers. This led to a wider region for the free-flowing liquid behavior, which we associated to with the formation of spherical nanoparticles as testified by the exemplary TEM micrograph in Figure 4c and, in turn, a narrower portion characterized by precipitated polymer. It is worth highlighting that, based on the concept of packing parameter, higher-order morphologies (*e.g.*, vesicles, bilayer structures) would have been expected for such asymmetric block copolymers. Apparently, important kinetic limitations prevent the nano-objects from reaching the most thermodynamically favored morphology, so that a wide region of spherical nanoparticles was actually observed.

The spherical NPs formed in the region of low solid content were extensively characterized via DLS, to relate the main colloidal properties to the structural parameters of the constituting block copolymers. This analysis confirmed a narrow particle size distribution for all the samples (PDI < 0.22 for samples at $T < T_{cp}$ as shown in Table S4), whose volume-average diameter linearly increases with p (Figure 5). The narrow distribution further confirms the actual formation of isotropic particles. In addition, the linear increase in the NP size with the length of the core-forming block can be predicted by eq 2, which was already demonstrated in our group for different systems and further supports the evidence of spherical nano-objects.[48]

https://doi.org/10.1021/acsapm.2c01598
ACS Appl. Polym. Mater. 2023, 5, 494−503

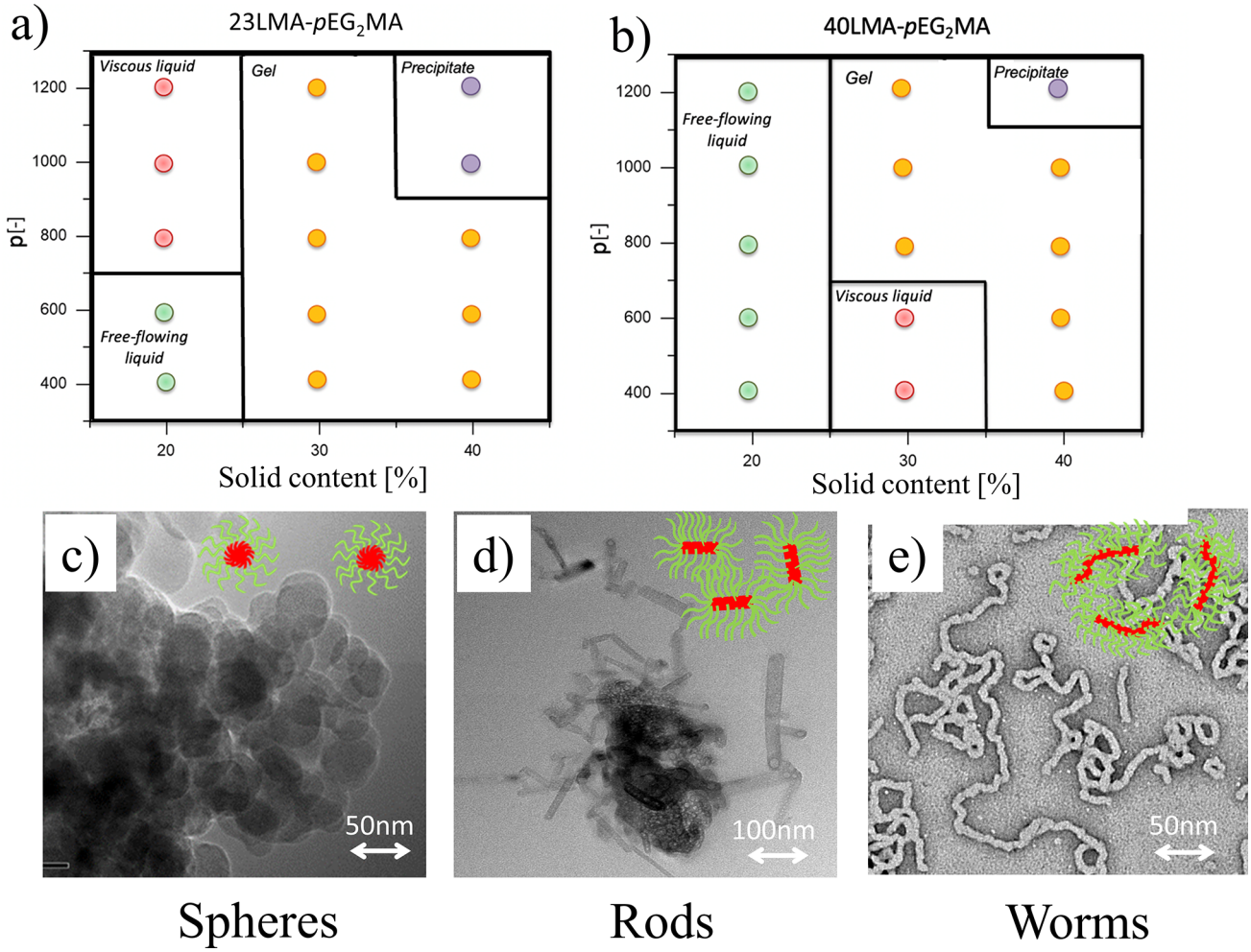

Figure 4. Phase diagram for the (a) 23LMA-pEG2MA samples and (b) 40LMA-pEG$_2$MA copolymers at a fixed temperature of 25 °C. (c) TEM micrograph of the sample 40LMA-600EG$_2$MA at 20% w/w solid content, which shows a free-flowing liquid behavior. (d) TEM micrograph of the sample 40LMA-600EG$_2$MA at 30% w/w solid content, which shows a viscous liquid behavior. (e) TEM micrograph of the sample 40LMA-600EG$_2$MA at 40% w/w solid content, which shows a self-standing gel behavior.

$$d = \frac{6 \times p \times M_{\mathrm{EG2MA}}}{A_{\mathrm{cov}} \times N_{\mathrm{av}} \times \rho_{\mathrm{EG2MA}}} \quad (2)$$

Here, ρ_{EG2MA} is the density of the poly(EG$_2$MA) segment, N_{av} is the Avogadro number, and A_{cov} is the area of the nanoparticle surface covered by a single stabilizing block.

To assess how the NP size is influenced by changing the temperature, all the samples were analyzed via DLS at 25 and 90 °C, representative of the conditions below and above their T_{cp}. Figure 5a,b demonstrates once more the UCST behavior of these copolymers. Indeed, the block copolymers self-assemble into nanoparticles whose size sharply decreases above the cloud point, as a result of the increased solubility of the thermoresponsive block in dectol. Given this increased solubility, the actual p contributing to the realization of the core of the NPs decreases, while the colloidal stability increases. Both these aspects determined a reduction in the average size, which can still be described according to eq 2. At both temperatures, the PDI is below 0.2, suggesting the presence of isotropic spherical nanoparticles. When overcoming the cloud point, a decrease in this parameter was experienced as well, confirming the increased solubility of the thermoresponsive segment of the copolymer.

In addition, it could be observed that the nanoparticle size has a clear dependence on both n and p, independently of the temperature chosen (25 or 90 °C). For fixed values of n, an increase in the number of repeating units in the thermoresponsive block leads to a linear increase in the nanoparticle size, with a more pronounced slope in the case of copolymers with a short stabilizer block (Figure 5c). In the same direction, by keeping p constant, the size of the nanoparticles has an inverse dependence on n. Both these behaviors agree with the predictions of eq 2 under the hypothesis that the stabilizer block disposes tangentially to the nanoparticle surface. Under this circumstance, the coverage area (A_{cov}) was demonstrated to be a linear function of the repeating units in the macroCTA, n in this case. As such, a longer macroCTA covers a larger portion of the NP surface, thus reducing their average size.

At higher solid contents, the copolymer morphology depends on the number of EG$_2$MA units, as evident from a visual inspection of the samples (see Figure S6). For low values of p (<600) and solid content, viscous and cloudy dispersions were experienced, while the formation of a self-standing gel can be appreciated by increasing the solid content and p.

The increase of the viscosity of the liquid is due to the rearrangement of the nanoparticles into rod-like particles, as can

https://doi.org/10.1021/acsapm.2c01598
ACS Appl. Polym. Mater. 2023, 5, 494−503

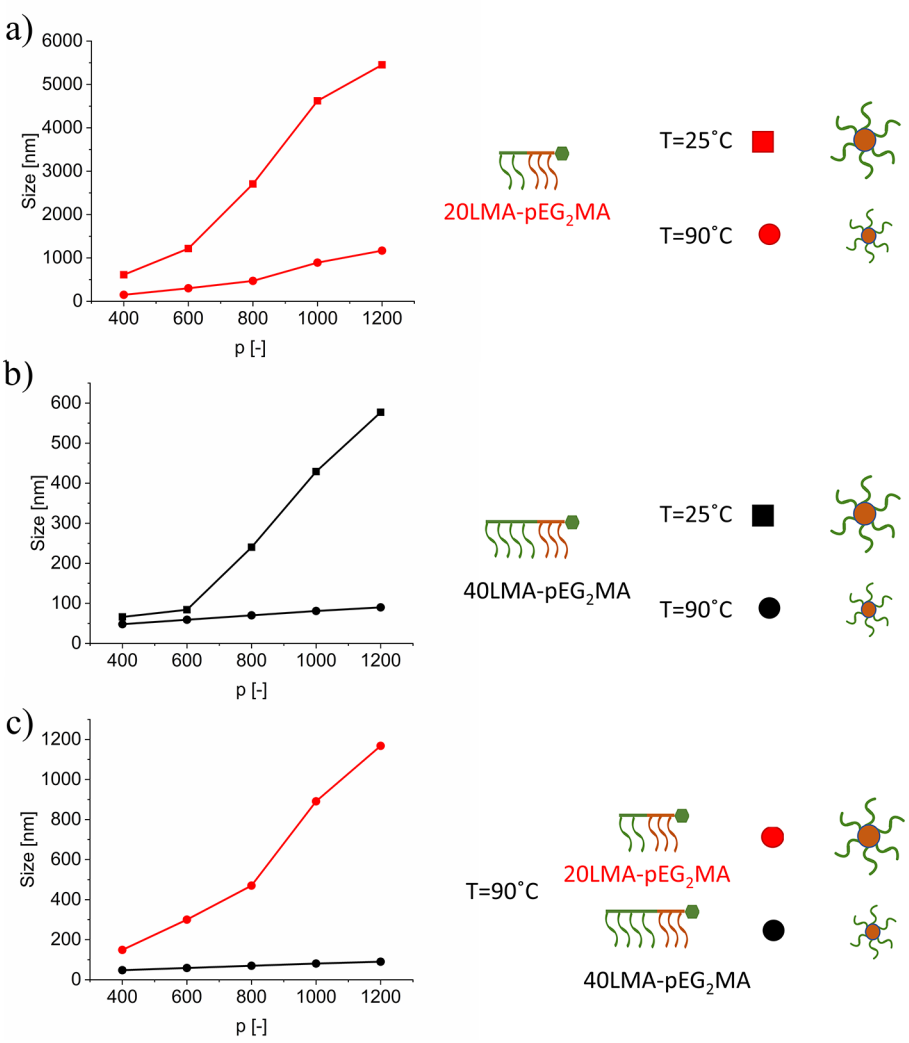

Figure 5. Volume-average size of the NPs formed by the block copolymers in dectol as a function of three parameters: *n*, *p*, and temperature. While *p* is shown on the *x* axis, the other two parameters are represented by using different colors (red for $n = 20$ or black for $n = 40$) or symbols (squares for $T = 25$ °C, below the cloud point, or circles for $T = 90$ °C, above the cloud point). (a) Comparison between copolymers with the same *n* (23LMA-pEG2MA) at two different temperatures, 25 and 90 °C; (b) comparison between copolymers with the same *n* (40LMA-pEG2MA) at two different temperatures, 25 and 90 °C; (c) comparison between copolymers with different *n* (23LMA-pEG2MA and 40LMA-pEG$_2$MA) at 90 °C, above the cloud point, where the thermoresponsive block is more solvophilic.

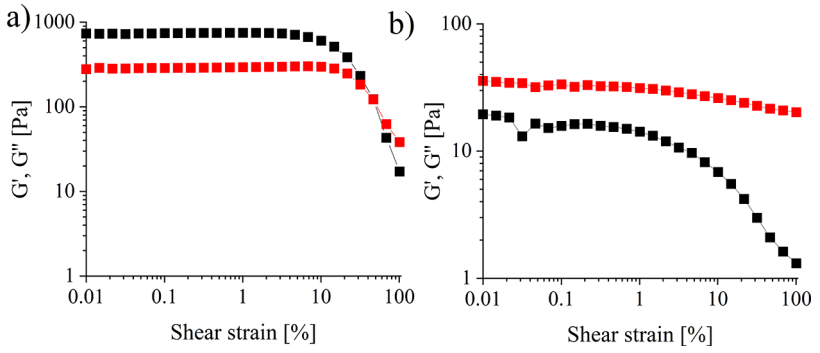

Figure 6. G' (black squares) and G'' (red squares) for the 23LMA-600EG$_2$MA 30% gel sample at increasing shear strains: (a) behavior at $T = 25$ °C; (b) behavior at $T = 90$ °C.

be observed in the TEM micrograph of the sample 40LMA-600EG$_2$MA at 30% w/w (Figure 4d).

On the other hand, the gelation of the system was ascribed to a worm-like morphology for the nano-objects produced in dectol, as confirmed by the TEM micrograph reported in Figure 4e for the sample 40LMA-600EG$_2$MA at 40% w/w, as an example. Moving to higher values of *p*, this gel phase appears also at lower solid content, due to the larger core-forming block. However, once the solid content is further increased, the system becomes more and more unstable until it precipitates out of dectol.

https://doi.org/10.1021/acsapm.2c01598
ACS Appl. Polym. Mater. 2023, 5, 494−503

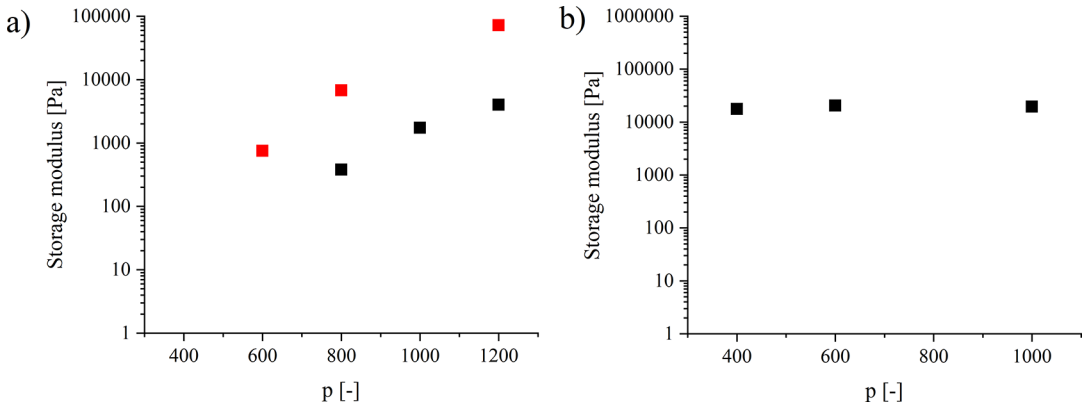

Figure 7. Storage modulus G' as a function of p for different copolymers. (a) Comparison between 23LMA-pEG$_2$MA 30% w/w (red squares) and 40LMA-pEG$_2$MA 30% w/w (black squares). (b) Trend for the 40LMA-pEG$_2$MA copolymers at 40% w/w solid content.

The rheological behavior of the samples in the gel region was characterized through a strain sweep test performed at 25 and 90 °C, to highlight their response to changes in temperature. The results from the sample 23LMA-600EG$_2$MA 30% w/w are shown in Figure 6, as an example.

At 25 °C, the storage modulus (G') is greater than the loss modulus (G'') for shear strains lower than 50%. This suggests a viscoelastic behavior for low strains, reflected in the gel appearance at room temperature. A shear-induced degelation can then be appreciated for this sample, with G'' overcoming G' at 50% shear strain (Figure 6a). On the other hand, when the temperature is increased above the T_{cp}, the copolymer becomes liquid as testified by G'' being higher than G' in the whole range of shear strains considered (Figure 6b). Therefore, this analysis confirms the possibility of synthesizing copolymers with a temperature-induced sol/gel transition in a non-polar medium like dectol and to exploit this interesting feature in different contexts, from lubricants to oil extraction.

To demonstrate how the rheology of these temperature-induced gels can be modulated by acting on the copolymer microstructure, G' measured at 25 °C and 1% shear strain was related to the number of thermoresponsive repeating units (p) and solid content (Figure 7).

It is possible to observe that the storage modulus grows monotonically with p for both the 23LMA-pEG$_2$MA 30% w/w and 40LMA-pEG$_2$MA 30% w/w copolymers (Figure 7a), suggesting the possible modulation of the rheological properties of the gel by acting on the length of the thermoresponsive portion. It is then worth highlighting that G' is always smaller for the samples produced from the 40LMA macroCTA than for those obtained from the 23LMA. This can be ascribed to the higher colloidal stability offered by the longer oleophilic block, responsible for a reduction in the length of the worm-like particles formed at 25 °C.

However, the influence of the length of the thermoresponsive block seems to become less relevant when the solid content is increased to 40% w/w, as the samples show nearly the same storage moduli independently of the value of p (Figure 7b).

Overall, the physicochemical properties and the thermoresponsive behavior of the synthesized copolymers either in the form of a suspension of NPs or as gels can be tuned by precisely controlling the solid content and the length of both the poly(LMA) block and the thermoresponsive block exploiting the living feature of RAFT polymerization. This allows the synthesis of modular diblock copolymers in a non-polar solvent like dectol, thus paving the way to applications in hydrocarbon blends commonly used in the oil & gas industry.

4. CONCLUSIONS

In this work, we studied the properties and thermoresponsive behavior of a library of well-defined diblock copolymers produced via RAFT dispersion polymerization in the non-polar solvent dectol. This technique allowed for finely controlling the length of the solvophilic poly(LMA) block n and that of the thermoresponsive poly(EG$_2$MA) block p, in addition to the copolymer dry content.

It was found that the cloud point of the system linearly increases with the number of thermoresponsive units. This parameter, together with the dry content, strongly influences also the morphology of the nano-objects produced in dectol. Spheres and worms could be obtained in specific regions of the p vs dry content phase diagram when the temperature was decreased below the T_{cp}. A good control over the thermoresponsive behavior can be then accessed with these modular copolymers. In addition, the region of pure worms is particularly interesting because it leads to the gelation of the system. The rheological behavior of these gels can be finely controlled by acting on the microstructure of the constituent copolymers. Therefore, these block copolymers can be conveniently employed when on-demand thickening or sol−gel transitions by lowering the environmental temperature are required.

■ ASSOCIATED CONTENT

Supporting Information

The Supporting Information is available free of charge at https://pubs.acs.org/doi/10.1021/acsapm.2c01598.

GPC and NMR characterizations of the macroCTAs and of the block copolymers, the summary of the properties of the different copolymers synthesized at different solid content, the average size and polydispersity of the spherical NPs synthesized and the visualization of the four behaviors used to generate the phase diagrams (PDF)

■ AUTHOR INFORMATION

Corresponding Author

Mattia Sponchioni − *Department of Chemistry, Materials and Chemical Engineering "Giulio Natta", Politecnico di Milano, 20131 Milano, Italy;* orcid.org/0000-0002-8130-6495; Email: mattia.sponchioni@polimi.it

https://doi.org/10.1021/acsapm.2c01598
ACS Appl. Polym. Mater. 2023, 5, 494−503

Authors

Gianmaria Gardoni − *Department of Chemistry, Materials and Chemical Engineering "Giulio Natta", Politecnico di Milano, 20131 Milano, Italy*

Nicolò Manfredini − *Department of Chemistry, Materials and Chemical Engineering "Giulio Natta", Politecnico di Milano, 20131 Milano, Italy*

Mattia Monzani − *Department of Chemistry, Materials and Chemical Engineering "Giulio Natta", Politecnico di Milano, 20131 Milano, Italy*

Davide Moscatelli − *Department of Chemistry, Materials and Chemical Engineering "Giulio Natta", Politecnico di Milano, 20131 Milano, Italy;* orcid.org/0000-0003-2759-9781

Complete contact information is available at: https://pubs.acs.org/10.1021/acsapm.2c01598

Author Contributions

G.G. − Investigation, Data Curation, Writing − Original draft; N.M. − Investigation, Data Curation; M.M. − Validation; M.S. − Conceptualization, Supervision, Writing − Review and editing; D.M. − Funding acquisition. All authors have read and given approval to the final version of the manuscript.

Notes

The authors declare no competing financial interest.

REFERENCES

(1) Fonseca, G. E.; McKenna, T. F.; Dubé, M. A. Miniemulsion vs. Conventional Emulsion Polymerization for Pressure-Sensitive Adhesives Production. *Chem. Eng. Sci.* **2010**, *65* (9), 2797−2810.

(2) Aguirre, M.; Hamzehlou, S.; González, E.; Leiza, J. R.Renewable Feedstocks in Emulsion Polymerization: Coating and Adhesive Applications. In *Advances in Chemical Engineering;*Elsevier Inc., 2020; Vol. *56*, pp 139−186. DOI: 10.1016/bs.ache.2020.07.004.

(3) Lin, Z.; Goddard, J. M. Photocurable Coatings Prepared by Emulsion Polymerization Present Chelating Properties. *Colloids Surf., B* **2018**, *172*, 143−151.

(4) Penfold, N. J. W.; Yeow, J.; Boyer, C.; Armes, S. P. Emerging Trends in Polymerization-Induced Self-Assembly. *ACS Macro Lett.* **2019**, *8* (8), 1029−1054.

(5) Sponchioni, M.Polymeric Nanoparticles for Controlled Drug Delivery. In *Nanomaterials for Theranostics and Tissue Engineering;*Rossi, F., Rainer, A., Eds.; Elsevier, 2020; pp 1−28. DOI: 10.1016/B978-0-12-817838-6.00001-2.

(6) van Mastrigt, F.; Stoffelsma, T.; Wever, D. A. Z.; Picchioni, F. Thermoresponsive Comb Polymers as Thickeners for High Temperature Aqueous Fluids. *Mater. Today Commun.* **2017**, *10*, 34−40.

(7) Manfredini, N.; Merigo, M.; Ilare, J.; Sponchioni, M.; Moscatelli, D. Limonene-in-Water Pickering Emulsion and on-Demand Separation Using Thermo-Responsive Biodegradable Nanoparticles. *Nanoscale* **2021**, *13* (18), 8543−8554.

(8) Moad, G.; Rizzardo, E. A 20th Anniversary Perspective on the Life of RAFT (RAFT Coming of Age). *Polym. Int.* **2020**, *69* (8), 658−661.

(9) Perrier, S. 50th Anniversary Perspective : RAFT Polymerization—A User Guide. *Macromolecules* **2017**, *50* (19), 7433−7447.

(10) Sponchioni, M.; Capasso Palmiero, U.; Manfredini, N.; Moscatelli, D. RAFT Copolymerization of Oppositely Charged Monomers and Its Use to Tailor the Composition of Nonfouling Polyampholytes with an UCST Behaviour. *React. Chem. Eng.* **2019**, *4* (2), 436−446.

(11) Fielding, L. A.; Derry, M. J.; Ladmiral, V.; Rosselgong, J.; Rodrigues, A. M.; Ratcliffe, L. P. D.; Sugihara, S.; Armes, S. P. RAFT Dispersion Polymerization in Non-Polar Solvents: Facile Production of Block Copolymer Spheres, Worms and Vesicles in n-Alkanes. *Chem. Sci.* **2013**, *4* (5), 2081.

(12) Zanoni, A.; Gardoni, G.; Sponchioni, M.; Moscatelli, D. Valorisation of Glycerol and CO2 to Produce Biodegradable Polymer Nanoparticles with a High Percentage of Bio-Based Components. *J. CO2 Util.* **2020**, *40*, 101192.

(13) D'Agosto, F.; Rieger, J.; Lansalot, M. RAFT-Mediated Polymerization-Induced Self-Assembly. *Angew. Chemie Int. Ed.* **2020**, *59* (22), 8368−8392.

(14) Sponchioni, M.; Ferrari, R.; Morosi, L.; Moscatelli, D. Influence of the Polymer Structure over Self-Assembly and Thermo-Responsive Properties: The Case of PEG-b-PCL Grafted Copolymers via a Combination of RAFT and ROP. *J. Polym. Sci., Part A: Polym. Chem.* **2016**, *54* (18), 2919−2931.

(15) Warren, N. J.; Mykhaylyk, O. O.; Mahmood, D.; Ryan, A. J.; Armes, S. P. RAFT Aqueous Dispersion Polymerization Yields Poly(Ethylene Glycol)-Based Diblock Copolymer Nano-Objects with Predictable Single Phase Morphologies. *J. Am. Chem. Soc.* **2014**, *136* (3), 1023−1033.

(16) Cao, P.-F.; Mangadlao, J. D.; Advincula, R. C. Stimuli-Responsive Polymers and Their Potential Applications in Oil-Gas Industry. *Polym. Rev.* **2015**, *55* (4), 706−733.

(17) Sponchioni, M.; Manfredini, N.; Zanoni, A.; Scibona, E.; Morbidelli, M.; Moscatelli, D. Readily Adsorbable Thermoresponsive Polymers for the Preparation of Smart Cell-Culturing Surfaces on Site. *ACS Biomater. Sci. Eng.* **2020**, *6* (9), 5337−5345.

(18) Lahasky, S. H.; Hu, X.; Zhang, D. Thermoresponsive Poly(α-Peptoid)s: Tuning the Cloud Point Temperatures by Composition and Architecture. *ACS Macro Lett.* **2012**, *1* (5), 580−584.

(19) Bordat, A.; Boissenot, T.; Nicolas, J.; Tsapis, N. Thermoresponsive Polymer Nanocarriers for Biomedical Applications. *Adv. Drug Delivery Rev.* **2019**, *138*, 167−192.

(20) Abulateefeh, S. R.; Spain, S. G.; Aylott, J. W.; Chan, W. C.; Garnett, M. C.; Alexander, C. Thermoresponsive Polymer Colloids for Drug Delivery and Cancer Therapy. *Macromol. Biosci.* **2011**, *11* (12), 1722−1734.

(21) Sponchioni, M.; Capasso Palmiero, U.; Moscatelli, D. Thermo-Responsive Polymers: Applications of Smart Materials in Drug Delivery and Tissue Engineering. *Mater. Sci. Eng., C* **2019**, *102*, 589−605.

(22) Halperin, A.; Kröger, M.; Winnik, F. M. Poly(N-Isopropylacrylamide) Phase Diagrams: Fifty Years of Research. *Angew. Chemie, Int. Ed.* **2015**, *54* (51), 15342−15367.

(23) Alarcon, C. d. l. H.; Pennadam, S.; Alexander, C. Stimuli Responsive Polymers for Biomedical Applications. *Chem. Soc. Rev.* **2005**, *34* (3), 276−285.

(24) Antonietti, M.; Förster, S. Vesicles and Liposomes: A Self-Assembly Principle Beyond Lipids. *Adv. Mater.* **2003**, *15* (16), 1323−1333.

(25) Jia, Z.; Monteiro, M. J. Temperature-Induced Gels from Worms Made by RAFT-Mediated Emulsion Polymerization. *Controlled Radical Polymerization: Materials* **2015**, *1188*, 79−90.

(26) Hunter, S. J.; Lovett, J. R.; Mykhaylyk, O. O.; Jones, E. R.; Armes, S. P. Synthesis of Diblock Copolymer Spheres, Worms and Vesicles via RAFT Aqueous Emulsion Polymerization of Hydroxybutyl Methacrylate. *Polym. Chem.* **2021**, *12* (25), 3629−3639.

(27) Sponchioni, M.; Rodrigues Bassam, P.; Moscatelli, D.; Arosio, P.; Capasso Palmiero, U. Biodegradable Zwitterionic Nanoparticles with Tunable UCST-Type Phase Separation under Physiological Conditions. *Nanoscale* **2019**, *11* (35), 16582−16591.

(28) Capasso Palmiero, U.; Sponchioni, M.; Manfredini, N.; Maraldi, M.; Moscatelli, D. Strategies to Combine ROP with ATRP or RAFT Polymerization for the Synthesis of Biodegradable Polymeric Nanoparticles for Biomedical Applications. *Polym. Chem.* **2018**, *9* (30), 4084−4099.

(29) Fielding, L. A.; Lane, J. A.; Derry, M. J.; Mykhaylyk, O. O.; Armes, S. P. Thermo-Responsive Diblock Copolymer Worm Gels in Non-Polar Solvents. *J. Am. Chem. Soc.* **2014**, *136* (15), 5790−5798.

(30) Sponchioni, M.; Morosi, L.; Lupi, M.; Capasso Palmiero, U. Poly(HPMA)-Based Copolymers with Biodegradable Side Chains Able to Self Assemble into Nanoparticles. *RSC Adv.* **2017**, *7* (80), 50981−50992.

(31) Brotherton, E. E.; Hatton, F. L.; Cockram, A. A.; Derry, M. J.; Czajka, A.; Cornel, E. J.; Topham, P. D.; Mykhaylyk, O. O.; Armes, S. P.

In Situ Small-Angle X-Ray Scattering Studies During Reversible Addition−Fragmentation Chain Transfer Aqueous Emulsion Polymerization. *J. Am. Chem. Soc.* **2019**, *141* (34), 13664−13675.
(32) Ratcliffe, L. P. D.; Derry, M. J.; Ianiro, A.; Tuinier, R.; Armes, S. P. A Single Thermoresponsive Diblock Copolymer Can Form Spheres, Worms or Vesicles in Aqueous Solution. *Angew. Chemie Int. Ed.* **2019**, *58* (52), 18964−18970.
(33) Le, D.; Keller, D.; Delaittre, G. Reactive and Functional Nanoobjects by Polymerization-Induced Self-Assembly. *Macromol. Rapid Commun.* **2019**, *40* (2), 1800551.
(34) Parkinson, S.; Hondow, N. S.; Conteh, J. S.; Bourne, R. A.; Warren, N. J. All-Aqueous Continuous-Flow RAFT Dispersion Polymerisation for Efficient Preparation of Diblock Copolymer Spheres, Worms and Vesicles. *React. Chem. Eng.* **2019**, *4* (5), 852−861.
(35) Gibson, R. R.; Fernyhough, A.; Musa, O. M.; Armes, S. P. Synthesis of Well-Defined Diblock Copolymer Nano-Objects by RAFT Non-Aqueous Emulsion Polymerization of N -(2-Acryloyloxy)Ethyl Pyrrolidone in Non-Polar Media. *Polym. Chem.* **2021**, *12* (26), 3762−3774.
(36) Pei, Y.; Thurairajah, L.; Sugita, O. R.; Lowe, A. B. RAFT Dispersion Polymerization in Nonpolar Media: Polymerization of 3-Phenylpropyl Methacrylate in n -Tetradecane with Poly(Stearyl Methacrylate) Homopolymers as Macro Chain Transfer Agents. *Macromolecules* **2015**, *48* (1), 236−244.
(37) Docherty, P. J.; Derry, M. J.; Armes, S. P. RAFT Dispersion Polymerization of Glycidyl Methacrylate for the Synthesis of Epoxy-Functional Block Copolymer Nanoparticles in Mineral Oil. *Polym. Chem.* **2019**, *10* (5), 603−611.
(38) György, C.; Hunter, S. J.; Girou, C.; Derry, M. J.; Armes, S. P. Synthesis of Poly(Stearyl Methacrylate)-Poly(2-Hydroxypropyl Methacrylate) Diblock Copolymer Nanoparticles via RAFT Dispersion Polymerization of 2-Hydroxypropyl Methacrylate in Mineral Oil. *Polym. Chem.* **2020**, *11* (28), 4579−4590.
(39) Cornel, E. J.; Smith, G. N.; Rogers, S. E.; Hallett, J. E.; Growney, D. J.; Smith, T.; O'Hora, P. S.; van Meurs, S.; Mykhaylyk, O. O.; Armes, S. P. Time-Resolved Small-Angle Neutron Scattering Studies of the Thermally-Induced Exchange of Copolymer Chains between Spherical Diblock Copolymer Nanoparticles Prepared via Polymerization-Induced Self-Assembly. *Soft Matter* **2020**, *16* (15), 3657−3668.
(40) Day, D. M.; Hutchings, L. R. The Self-Assembly and Thermoresponsivity of Poly(Isoprene-b-Methyl Methacrylate) Copolymers in Non-Polar Solvents. *Eur. Polym. J.* **2021**, *156*, 110631.
(41) Blesic, M.; Dichiarante, V.; Milani, R.; Linder, M.; Metrangolo, P. Evaluating the Potential of Natural Surfactants in the Petroleum Industry: The Case of Hydrophobins. *Pure Appl. Chem.* **2018**, *90* (2), 305−314.
(42) Meng, J.; Sontti, S. G.; Sadeghi, M.; Arends, G. F.; Nikrityuk, P.; Tan, X.; Zhang, X. Size Distribution of Primary Submicron Particles and Larger Aggregates in Solvent-Induced Asphaltene Precipitation in a Model Oil System. *Fuel* **2022**, *322*, 124057.
(43) Pasparakis, G.; Tsitsilianis, C. LCST Polymers: Thermoresponsive Nanostructured Assemblies towards Bioapplications. *Polymer* **2020**, *211* (July), 123146.
(44) Badi, N. Non-Linear PEG-Based Thermoresponsive Polymer Systems. *Prog. Polym. Sci.* **2017**, *66*, 54−79.
(45) Tkachenko, V.; Matei Ghimbeu, C.; Vaulot, C.; Vidal, L.; Poly, J.; Chemtob, A. RAFT-Photomediated PISA in Dispersion: Mechanism, Optical Properties and Application in Templated Synthesis. *Polym. Chem.* **2019**, *10* (18), 2316−2326.
(46) Blanazs, A.; Madsen, J.; Battaglia, G.; Ryan, A. J.; Armes, S. P. Mechanistic Insights for Block Copolymer Morphologies: How Do Worms Form Vesicles? *J. Am. Chem. Soc.* **2011**, *133* (41), 16581−16587.
(47) Colombo, C.; Dragoni, L.; Gatti, S.; Pesce, R. M.; Rooney, T. R.; Mavroudakis, E.; Ferrari, R.; Moscatelli, D. Tunable Degradation Behavior of PEGylated Polyester-Based Nanoparticles Obtained Through Emulsion Free Radical Polymerization. *Ind. Eng. Chem. Res.* **2014**, *53* (22), 9128−9135.
(48) Palmiero, U. C.; Agostini, A.; Gatti, S.; Sponchioni, M.; Valenti, V.; Brunel, L.; Moscatelli, D. RAFT Macro-Surfmers and Their Use in the Ab Initio RAFT Emulsion Polymerization To Decouple Nanoparticle Size and Polymer Molecular Weight. *Macromolecules* **2016**, *49* (22), 8387−8396.

https://doi.org/10.1021/acsapm.2c01598
ACS Appl. Polym. Mater. 2023, 5, 494−503